

Ionization probabilities of Ne, Ar, Kr, and Xe by proton impact for different initial states and impact energies

J. E. Miraglia^{a,b}, C. C. Montanari^{a,b,*}

^a*Instituto de Astronomía y Física del Espacio,
Consejo Nacional de Investigaciones Científicas y Técnicas and Universidad de Buenos Aires,
casilla de correo 67, sucursal 28, (C1428EGA) Buenos Aires, Argentina*
^b*Facultad de Ciencias Exactas y Naturales, Universidad de Buenos Aires
Buenos Aires, Argentina*

Abstract

Tables of *ab-initio* total cross sections, probabilities at zero impact parameter, and impact parameter moments are presented concerning the ionization of Ne, Ar, Kr, and Xe by proton impact in the energy range (0.1-10) MeV. The calculations correspond to the continuum distorted wave eikonal initial state approximation (CDW-EIS) for energies up to 1 MeV, and to the first Born approximation for larger energies. The results displayed in the tables are disaggregated for the different initial bound states, considering all the shells for Ne and Ar, the L-M-N shells of Kr and the M-N-O shells of Xe. Our inner-shell ionization cross sections are compared with the available experimental data and with the ECPSSR results.

arXiv:1606.02543v1 [physics.atom-ph] 8 Jun 2016

*Corresponding author.

Email address: mclaudia@iafe.uba.ar (C. C. Montanari)

Contents

1. Introduction	3
2. Total ionization cross sections	4
3. Inner-shell ionization	5
4. Ionization probabilities as a function of the impact parameter	7
5. Impact parameter moments	9
6. Conclusions	9
References	10
Explanation of Tables	13
Tables	
1. Total ionization cross sections, σ_{nlm} , of Neon K and L shells by 0.1-10 MeV protons. Atomic units are used. See page 13 for explanation.	16
2. Total ionization cross sections, σ_{nlm} , of Argon K, L and M shells by 0.1-10 MeV protons. Atomic units are used. See page 13 for explanation	16
3. Total ionization cross sections, σ_{nlm} , of Krypton L, M and N shells by 0.1-10 MeV protons. Atomic units are used. See page 13 for explanation.	16
4. Total ionization cross sections, σ_{nlm} , of Xenon M, N and O shells by 0.1-10 MeV protons. Atomic units are used. See page 13 for explanation.	16
5. Ionization probabilities at zero impact parameter of Neon K and L shells by 0.1-10 MeV protons. See page 14 for explanation.	17
6. Ionization probabilities at zero impact parameter of Argon K, L and M shells by 0.1-10 MeV protons. See page 14 for explanation.	17
7. Ionization probabilities at zero impact parameter of Krypton M and N shells by 0.1-10 MeV protons. See page 14 for explanation.	17
8. Ionization probabilities at zero impact parameter of Xenon N and O shells by 0.1-10 MeV protons. See page 14 for explanation.	17
9. Mean radii $\langle r_{nl} \rangle$ of the atomic nl subshells of Ne, Ar, Kr and Xe (in atomic units).	17
10. Impact parameter moment of order -1 , $\langle b_{nlm}^{-1} \rangle$ for proton impact in Ne, normalized to the inverse of the mean radius of each subshell, $\langle r_{nl} \rangle^{-1}$. See page 14 for explanation.	18
Impact parameter moment of order -1 , $\langle b_{nlm}^{-1} \rangle$, for proton impact in Ar, normalized to the inverse of the mean radius of each subshell, $\langle r_{nl} \rangle^{-1}$. See page 14 for explanation.	18
12. Impact parameter moment of order -1 , $\langle b_{nlm}^{-1} \rangle$, for proton impact in Kr, normalized to the inverse of the mean radius of each subshell, $\langle r_{nl} \rangle^{-1}$. See page 14 for explanation.	18
13. Impact parameter moment of order -1 , $\langle b_{nlm}^{-1} \rangle$, for proton impact in Xe, normalized to the inverse of the mean radius of each subshell, $\langle r_{nl} \rangle^{-1}$. See page 14 for explanation.	18
14. Mean impact parameter, $\langle b_{nlm}^1 \rangle$, for proton in Ne, normalized to the mean radius of each subshell, $\langle r_{nl} \rangle$. See page 14 for explanation.	19
15. Mean impact parameter, $\langle b_{nlm}^1 \rangle$, for proton in Ar, normalized to the mean radius of each subshell, $\langle r_{nl} \rangle$. See page 15 for explanation.	19
16. Mean impact parameter, $\langle b_{nlm}^1 \rangle$, for proton in Kr, normalized to the mean radius of each subshell, $\langle r_{nl} \rangle$. See page 15 for explanation.	19

17. Mean impact parameter, $\langle b_{nlm}^1 \rangle$, for proton in Xe, normalized to the mean radius of each subshell, $\langle r_{nl} \rangle$. See page 15 for explanation.	19
--------------------------------------------------------------------------------------------------------------------------------------------------------------------------------------------	----

1. Introduction

Ionization data, involving experimental and theoretical values, has received great attention for a very long time (see for example [1] and references therein). However, current progress of beam characterization methods, atomic analytical techniques such as the so-called extended particle induced x-ray emission (PIXE) [2, 3], and multiple-purpose simulations for the passage of particles through matter as the Geant4 [4], have aroused new interest and requirements of accurate data and reliable predictions, and have also shown certain vacancy areas for the theoretical development.

Reliable values for the probabilities as function of the impact parameter are the seeds to describe the total ionization cross sections of the different shells. But also, these probabilities are the inputs for the multiple ionization calculations in a multinomial combination of the impact parameter probabilities [5]. From the theoretical point of view, these probabilities represent a challenge and a test of the capability of a theory to describe wave functions and interaction potentials. Different approaches have been employed over the years, from the basic first Born approximation, to distorted wave methods, numerical solution of the Schrödinger equation or collective response models [6–11]. Moreover, in very recent works, the ionization probabilities by proton and antiproton impact have been the seeds to obtain multiple ionization cross sections of rare gases by electron and positron impact, with reasonably good results [12, 13]. It is worth to note that multiple ionization cross sections are highly dependent on the inner-shell ionization probabilities, which contribute to the final values through Auger-type processes [8, 12].

There are different compilations of experimental data for the total ionization cross sections of the K-shell [14, 15] and the L-shell [1, 16]. One of the most employed models for K and L-shell ionization cross sections is the ECPSSR by Brandt and Lapicki [17, 18], of high efficiency and the usual input in PIXE codes [19]. Instead, reliable values of M-shell ionization are scarce [20, 21]. This is due to the complexity of the M-X-ray spectra because of the existence of five subshells [22]. It is usual that the experimental data are presented as X-ray production cross sections. The conversion of the X-ray production cross sections to the total ionization cross sections depends on multiple ionization parameters and fluorescence yields. Different possible values are discussed [23, 24]; however, the current state of the experimental techniques [25, 26] and the advance in X-ray spectrometers represent an improvement on this respect [1].

The goal of the present tabulation is to make available *ab-initio* CDW-EIS and first Born approximation results for proton impact ionization of the heaviest rare gases, for the different subshells. Presents results are calculated as in [27–29], by rigorously solving the radial Schrödinger equation for different angular momenta for both the initial bound and the final continuum states. Thus, we can assure the proper description of the continuum wave function and its mathematical orthogonality to the bound state. These values have already been tested in total [27] and differential [28] ionization cross sections. Also the probabilities as function of the impact parameter have been employed in multiple ionization calculations [9, 12, 13, 30] with good agreement with the experimental data, even for sextuple ionization of

Kr (Xe), where L-shell (M-shell) contribution is decisive.

In the following sections we make available these CDW-EIS values for proton impact energies 0.1-1 MeV, and also the first Born approximation results for proton energies 1-10 MeV, considering the ionization of different subshells: Ne (1s, 2s, 2p), Ar (1s,..., 3p), Kr (2s,..., 4p) and Xe (3s,..., 5p). We display total ionization cross sections, probabilities at zero impact parameter, and impact parameter moments of order 1 and -1 . We also include the comparison of our inner-shell ionization cross sections with the available experimental data, and with the ECPSSR values [17], for the K-shell of Ne, K and L-shells of Ar, L and M-shells of Kr and M and N-shells of Xe. Atomic units are used throughout this work, except when specifically mentioned.

2. Total ionization cross sections

The total ionization cross section of an electron initially in the nlm state, due to the interaction with a heavy projectile of charge Z_P (in this work $Z_P = 1$, proton impact) and impact velocity v , is given by the four-dimension integral

$$\sigma_{nlm} = \frac{(2\pi)^2}{v^2} \int d\vec{k} \int d\vec{\eta} \left| T_{\vec{k},nlm}(\vec{\eta}) \right|^2 \quad (1)$$

where $T_{\vec{k},nlm}(\vec{\eta})$ is the transition matrix as a function of the momentum transferred $\vec{\eta}$ perpendicular to the incident velocity \vec{v} , and \vec{k} is the momentum of the emitted electron. For heavy projectiles such as protons, the integration over $\vec{\eta}$ extends to infinity.

If we are interested in high energy collisions, we can resort to the first Born approximation. This is a perturbative method valid at large impact velocities and low projectile charges, with the initial and final wave functions being the unperturbed ones. The first Born transition matrix element is given by

$$T_{\vec{k},nlm}^{Born}(\vec{\eta}) = \frac{1}{(2\pi)^{3/2}} \tilde{V}_P(p) \int d\vec{r} \varphi_{\vec{k}}^*(r) \exp(i \vec{p} \cdot \vec{r}) \varphi_{nlm}(r). \quad (2)$$

Here $\varphi_{\vec{k}}$ (φ_{nlm}) is the final (initial) continuum (bound) eigenfunction of the target hamiltonian; $\tilde{V}_P(p) = -\sqrt{2/\pi} Z_P/p^2$ is the Fourier transform of the projectile-electron Coulomb potential, and $\vec{p} = \vec{K}_i - \vec{K}_f$ is the momentum transferred, with \vec{K}_i (\vec{K}_f) being the initial (final) projectile momentum. The momentum transferred can also be expressed as $\vec{p} = (\vec{\eta}, p_m)$, with p_m being the minimum momentum transfer along the direction of \vec{v} , $p_m = (\varepsilon_f - \varepsilon_i)/v$, and ε_i (ε_f) the initial (final) electron energy.

If we are interested in the intermediate energy regime, i.e. proton energies smaller than 1 MeV, we have to improve the calculation of the transition matrix. To that end we resort to the rigorous calculations using the CDW-EIS approximation [27, 28]. This model, initially proposed by Crothers and McCann [31], is one of the most reliable approximations to deal with calculations of ionization probabilities in the intermediate to high energy regime [32, 33]. Within the CDW-EIS approach the distorted wave functions include the projectile distortion in the initial and final channels. The T-matrix element reads

$$T_{\vec{k},nlm}^{CDW-EIS}(\vec{\eta}) = -\frac{1}{(2\pi)^{3/2}} \vec{W}(\vec{p}) \cdot \vec{G}_{\vec{k},nlm}(\vec{p}), \quad (3)$$

with

$$\vec{G}_{\vec{k},nlm}(\vec{p}) = \int d\vec{r}' \left[\vec{\nabla} \varphi_{\vec{k}}(\vec{r}') \right]^* e^{i \vec{p} \cdot \vec{r}'} \varphi_{nlm}(\vec{r}'), \quad (4)$$

$$\vec{W}(\vec{p}) = N_\xi \int \frac{d\vec{r}'}{(2\pi)^{3/2}} E_{\vec{v}}^+(\vec{r}') e^{-i \vec{p} \cdot \vec{r}'} \vec{\nabla} F_{\vec{v}}^-(\vec{r}'), \quad (5)$$

$$E_{\vec{v}}^+(\vec{r}') = \exp[-i\xi \ln(v r + \vec{v} \cdot \vec{r}')], \quad (6)$$

$$F_{\vec{v}}^-(\vec{r}') = {}_1F_1(-i\xi, 1, -iv r - i\vec{v} \cdot \vec{r}'), \quad (7)$$

and

$$N_\xi = \exp(\xi/2)\Gamma(1 + i\xi), \quad (8)$$

where $\xi = Z_P/v$, and ${}_1F_1$ is the confluent hypergeometric. In our case, both φ_{nlm} and $\varphi_{\vec{k}}$ are numerical solutions of the same Hamiltonian, therefore fully orthogonal, then the transition matrix $T_{if}^{CDW-EIS}$ does not display prior-post discrepancies.

The initial bound and final continuum radial wave functions were obtained by using the RADIALF code developed by Salvat and co-workers [34]. The number of pivots used to solve the Schrödinger equation rounds a few thousands of points, depending on the number of oscillations of the continuum. The radial integration was performed using the cubic spline technique. The number of angular momenta considered, l_{\max} , varied between 8, at very low ejected-electron energies, up to 28, at the largest energies considered. The same number of azimuth angles were required to obtain the fourfold differential cross section (on \vec{k} and $\vec{\eta}$). Each total cross section σ_{nlm} in Eq. (1) was calculated using 35 to 199 momentum transfer values of η to determine a doubly differential cross section, 28 fixed electron angles and around 40 electron energies ($E = k^2/2$), depending on the projectile impact energy.

In tables 1-4 we report our results for proton impact total ionization cross sections of the four heaviest rare gases: Ne, Ar, Kr, and Xe. CDW-EIS values are displayed for impact energies 0.1-1 MeV, and the first Born approximation for 1-10 MeV. A comparison between them is possible at 1 MeV. In all these cases we show separately the contributions of the different nlm initial states, ranging from the valence shell to two deeper shells.

3. Inner-shell ionization

The total ionization cross sections are determined mainly by the outer target shells. The CDW-EIS and first Born approximation values presented here proved to be effective in the description of these total cross sections, as shown in [27]. On the other hand, the cross sections for highly ionized targets (i.e. triple ionization of Ar, quintuple ionization of Kr, sextuple ionization of Xe) strongly depend on inner-shell contributions due to Auger cascade processes [12, 30].

In order to examine further the theoretical values displayed in tables 1-4, in figures 1-4 we display these values in comparison with the experimental data available (only for the K and L-shells) and with the ECPSSR values obtained using the ISICS11 code by Cipolla [35] (we take note of the comments by Smit and Lapicki [36] about this code). To our knowledge, no measurements have been reported for the M-shell ionization of Kr and Xe, or the N-shell ionization of Xe by proton impact.

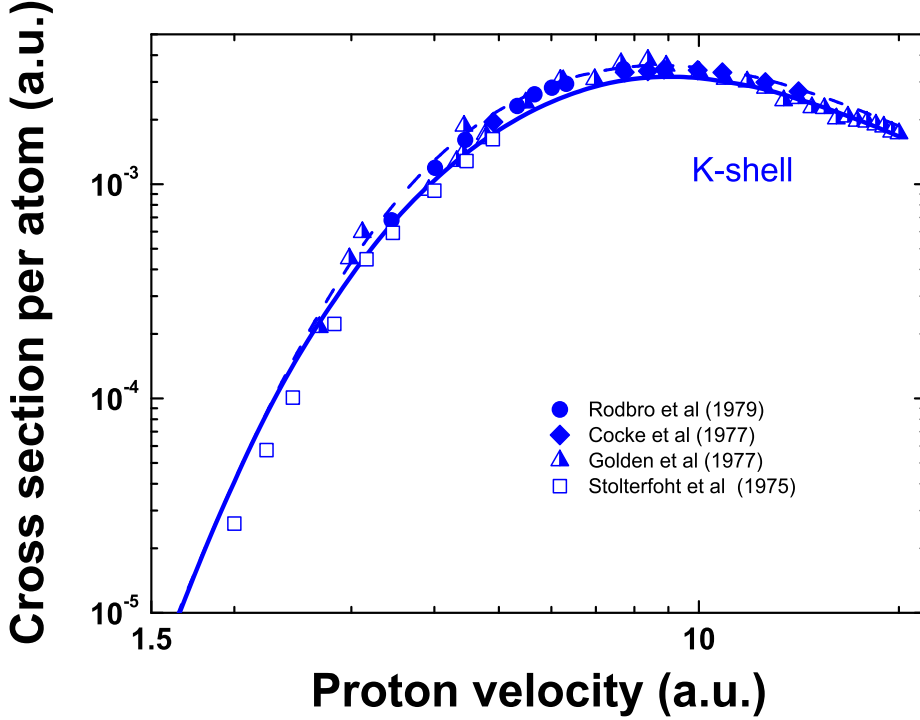


Fig. 1: K-shell ionization cross section of Ne by proton impact. Curves: solid line, present results displayed in table 1; dashed line, ECPSSR [17, 35]. Symbols: experimental data by Rodbro *et al* [37], Cocke *et al* [38], Golden *et al* [39], and Stolterfoht *et al* [40].

The K-shell ionization cross section displayed in figure 1 shows good agreement with the data. Note that for proton impact energy above 700 keV, the multiple ionization of Ne is sensitive to the K-shell ionization. It contributes directly to multiple ionization via single ionization of one K-shell electron followed by postcollisional electron emission via Auger processes. Similar importance has the L-shell of Ar displayed in figure 2. For this shell we include in figure 2 the proton impact data compiled by Miranda and Lapicki [1], and the deuteron impact data by Watson and Toburen [49]. For the ionization of Ar K-shell the agreement with the experiments and the ECPSSR is very good. For L-shell ionization, our description differs from the ECPSSR one, while the experimental data seems to be in between both curves.

Perhaps the most interesting feature is displayed in figure 3 for Kr. For L-shell ionization the agreement of the present results with the measurements by Winters *et al* [41] and Czuchlewski *et al* [42], and with the ECPSSR is very good. However, for M-shell ionization the situation is different: we got a clear discrepancy with the ECPSSR results [35] and no experimental data is available. Present M-shell ionization probabilities of Kr have already been employed in multiple ionization calculations with very good agreement with the experimental data [9, 30]. In triple and quadruple ionization of Kr at high energies the M-shell ionization plays a mayor role due to single ionization followed by Auger emission of 2 or more electrons. This is also a test of the present results validity.

Finally, in figure 4 we display the M and N-shell ionization cross sections of Xe. Good agreement with ECPSSR is observed for the M-shell ionization at high energies, and a clear difference below 500 keV. The M-shell of Xe is very important in quintuple and sextuple ionization above 1 MeV [12, 30], which is the region where both calculations agree

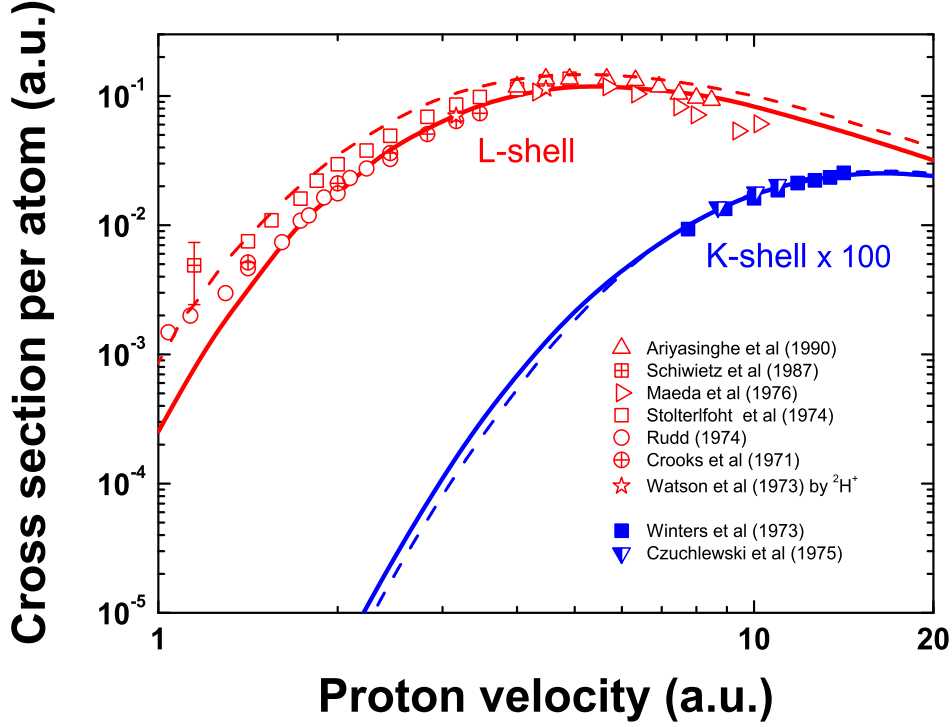


Fig. 2: K and L-shell ionization cross sections of Ar by proton impact. Curves: solid line, present results displayed in table 2; dashed line, ECPSSR [17, 35]. Symbols: K-shell experimental data by Winters *et al* [41], and by Czuchlewski *et al* [42]; L-shell experimental data by Ariyasinghe *et al* [43], Schiwietz *et al* [44], Maeda *et al* [45], Stolterfoht *et al* [46], Rudd [47], Crooks and Rudd [48], and Watson and Toburen [49] (deuteron impact).

well.

4. Ionization probabilities as a function of the impact parameter

The transition amplitude $a_{\vec{k},nlm}(\vec{b})$ as a function of the impact parameter \vec{b} is defined with the help of the bi-dimensional Fourier transform

$$a_{\vec{k},nlm}(\vec{b}) = \int d\vec{\eta} \frac{\exp(i\vec{b} \cdot \vec{\eta})}{2\pi} T_{\vec{k},nlm}(\vec{\eta}). \quad (9)$$

with the probability being $P_{\vec{k},nlm}(\vec{b}) = |a_{\vec{k},nlm}(\vec{b})|^2$. To solve (9) we expanded

$$T_{\vec{k},nlm}(\vec{\eta}) = \sum_{\mu=-M}^M i^{\mu} \frac{\exp(i\mu \varphi_{\eta})}{\sqrt{2\pi}} T_{\vec{k},nlm}^{(\mu)}(\eta). \quad (10)$$

where $\vec{\eta} = \{\eta, \varphi_{\eta}\}$. We integrated numerically the T-matrix elements for different angular momentum and added them appropriately. To be consistent, the maximum value M was considered to be the maximum angular momenta used to solve the Schrödinger equation. Special care should be taken to obtain $T_{\vec{k},nlm}^{(\mu)}(\eta)$ (see details in [9]). For practical purposes all these $T_{\vec{k},nlm}^{(\mu)}(\eta)$ values were stored in a large table of $(2 \times 8 + 1)$ to $(2 \times 28 + 1)$ values of μ , around 70 values of η , 28 electron angles Ω , and between 33 to 45 values of E , which are available upon request.

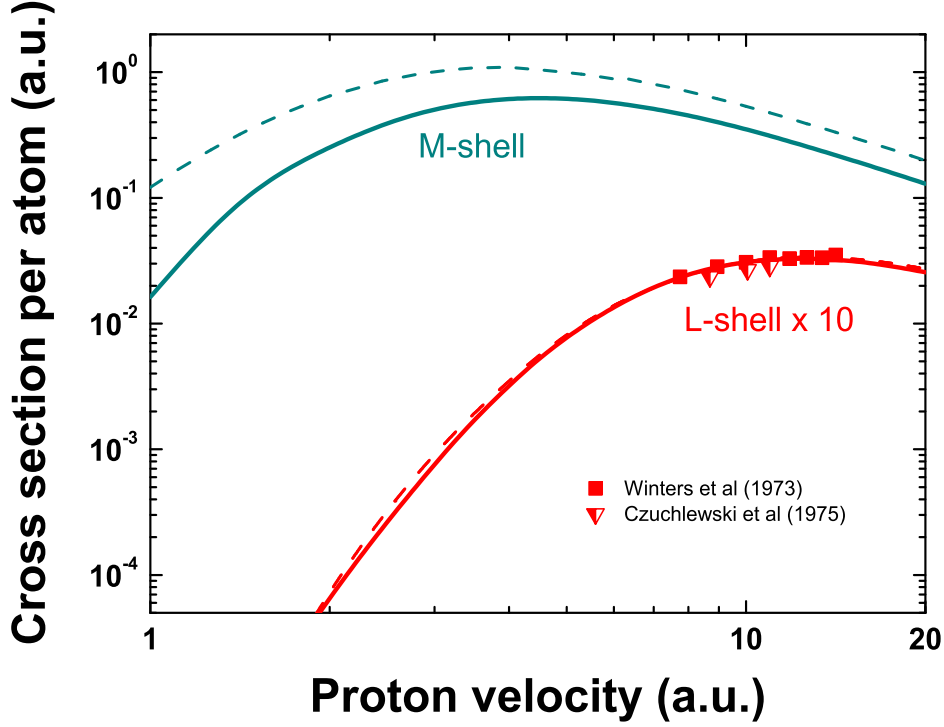


Fig. 3: L and M-shell ionization cross sections of Kr by proton impact. Curves: solid line, present results displayed in table 3; dashed line, ECPSR. Symbols: experimental data for L-shell ionization by Winters *et al* [41], and by Czuchlewski *et al* [42].

Afterwards, equation (9) can be written as

$$a_{\vec{k},nlm}(\vec{b}) = \sum_{\mu=-M}^M i^{\mu} \frac{\exp(i\mu \varphi_{\eta})}{\sqrt{2\pi}} a_{\vec{k},nlm}^{(\mu)}(b), \quad (11)$$

with

$$a_{\vec{k},nlm}^{(\mu)}(b) = i^{-\mu} \int_0^{\infty} d\eta \eta J_{\mu}(b\eta) T_{\vec{k},nlm}^{(\mu)}(\eta), \quad (12)$$

and with $J_{\mu}(b\eta)$ being the cylindrical Bessel function. Then the total ionization probability as a function of the impact parameter is obtained after integrating in the ejection electron space

$$P_{nlm}(\vec{b}) = \frac{1}{2\pi} \sum_{m=-M}^M \int d\vec{k} \left| a_{\vec{k},nlm}^{(\mu)}(b) \right|^2. \quad (13)$$

It is always convenient to re-calculate the total cross section as $\sigma_{nlm} = \int d\vec{b} P_{nlm}(\vec{b})$ to check the procedure.

These impact parameter dependent probabilities are very important because they are the seeds to get the different multiple ionization ones by introducing them in the multinomial expansion [6, 8]. If you are interested in multiple processes, the behaviour of the probability at small impact parameters happens to be very important. In tables 5-8 we display the geometrical factor $P_{nlm}(0)$ for the four rare gases, considering the different subshells and impact energies.

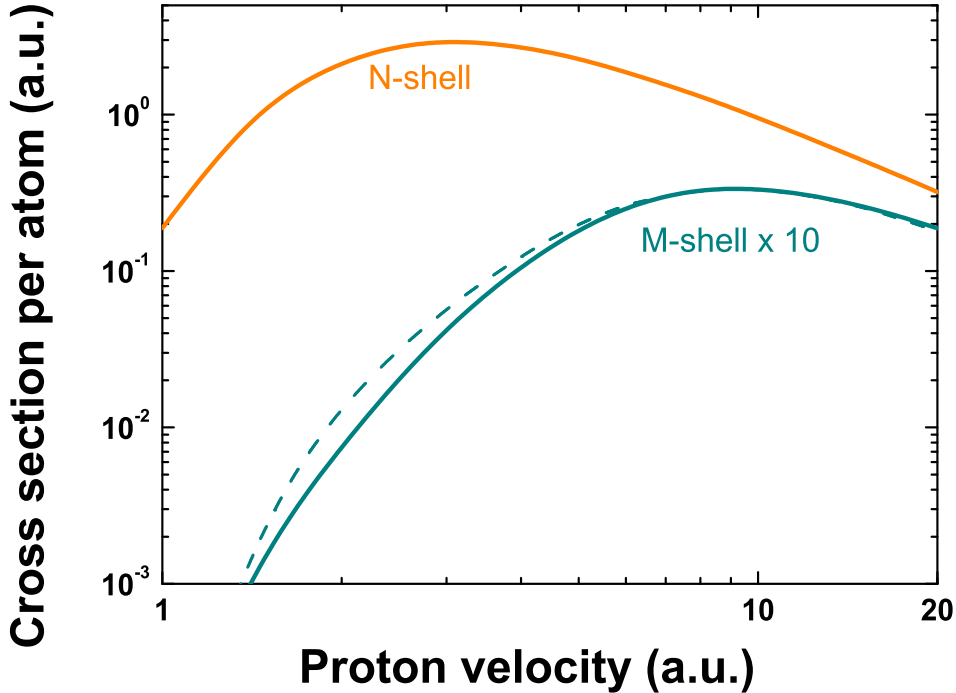


Fig. 4: M and N-shell ionization cross sections of Xe by proton impact. Curves: solid line, present results displayed in table 4; dashed line, ECPSR.

5. Impact parameter moments

We define the different impact parameter moments as

$$\langle b_{nlm}^J \rangle = \frac{1}{\sigma_{nlm}} \int d\vec{b} P_{nlm}(\vec{b}) \left(\frac{b}{\langle r_{nl} \rangle} \right)^J. \quad (14)$$

To bring these moments to unity, we have normalized to $\langle r_{nl} \rangle$, the mean radius of the initial atomic state (see Table 9). In Tables 10-17 we display $\langle b_{nlm}^1 \rangle$ and $\langle b_{nlm}^{-1} \rangle$ for Ne, Ar, Kr and Xe and different subshells. These are two important parameters, specially to compare with classical trajectory Monte Carlo calculations. The classical microcanonical ensemble, usually used to describe the initial state velocity distribution, has a finite space dimension. It produces $P(b)$ which falls down abruptly with b . Thus, total cross sections are generally well reproduced at expenses of an enhancement of $P(0)$. A comparison with our results on these two regions: $P(0)$ and $\langle b_{nlm}^1 \rangle$ can shed some light on the reliability of the approach.

6. Conclusions

We tabulated the results of *ab-initio* total cross sections, probabilities at zero impact parameter, and two impact parameter moments for ionization of Ne, Ar, Kr, and Xe by proton impact, using the CDW-EIS approximation for energies up to 1 MeV and the first Born approximation for higher energies, up to 10 MeV. We have considered all the shells of Ne and Ar, the L-M-N shells of Kr, and the M-N-O shells of Xe. In this way we have described the ionization

probability through four values: σ_{nlm} , $P_{nlm}(0)$, $\langle b_{nlm}^1 \rangle$ and $\langle b_{nlm}^{-1} \rangle$. Imposing these four conditions to a reasonable trial expression for $P_{nlm}(\vec{b})$ one can describe most of the physics involved, even for multiple ionization processes.

Acknowledgments

The authors acknowledge the financial support from the following Argentine institutions: Consejo Nacional de Investigaciones Científicas y Técnicas (CONICET), Universidad de Buenos Aires, through the programme UBACyT, and Agencia Nacional de Promoción Científica y Tecnológica (ANPCyT). They also thank Professors Javier Miranda and Gregory Lapicki for their interesting comments on this subject and for kindly sharing their tables of data.

References

- [1] J. Miranda and G. Lapicki, *At. Data Nucl. Data Tables* **100** (2014) 651-780.
- [2] S.A.E. Johansson, J.L. Campbell, K. Malmqvist (Eds.), *Particle Induced X-ray Spectrometry (PIXE)*, John Wiley & Sons, New York, 1995.
- [3] J. Ferraz Dias, L. Amaral and M. L. Yoneama (Eds.), *Proceedings of the 13th International Conference on Particle Induced X-ray Emission (PIXE 2013)*, *Nucl. Instrum. and Meth. Phys. Res. B* **318** (2014) 1-218.
- [4] M.G. Pia, G. Weidenspointner, M. Augelli, L. Quintieri, P. Saracco, M. Sudhakar, A. Zoglauer, *IEEE Trans. Nucl. Sci.* **56** (2009) 3614-3649; *J. Phys. Conf. Series* **219** (2010) 032018.
- [5] R.E. Olson, *J. Phys. B: At. Mol. Phys.* **12** (1979) 1843.
- [6] T. Spranger and T. Kirchner, *J. Phys. B: At. Mol. Opt. Phys.* **37** (2004) 4159.
- [7] E.G. Cavalcanti, G.M. Sigaud, E.C. Montenegro, M.M. Sant 'Anna, and H. Schmidt-Bocking, *J. Phys. B: At. Mol. Opt. Phys.* **35** (2002) 3937 .
- [8] C.C. Montanari, E.C. Montenegro and J. E. Miraglia, *J. Phys. B: At. Mol. Opt. Phys.* **43** (2010) 165201.
- [9] C.C. Montanari and J.E. Miraglia, *J. Phys. B: At. Mol. Opt. Phys.* **45** (2012) 105201.
- [10] M.E. Galassi, R.D. Rivarola, and P.D Fainstein, *Phys. Rev. A* **75** (2007) 052708.
- [11] C.D. Archubi, C.C. Montanari, J.E. and Miraglia, *J. Phys. B: At. Mol. Opt. Phys.* **40** (2007) 943.
- [12] C.C. Montanari, J.E. Miraglia, *J. Phys. B: At. Mol. Opt. Phys.* **47** (2015) 105203.
- [13] C.C. Montanari, J.E. Miraglia, *J. Phys. B: At. Mol. Opt. Phys.* **48** (2014) 165203.
- [14] H. Paul, *Nucl. Instrum. Meth.* **192** (1982) 11-24. Also at <http://www.exphys.jku.at/Kshells/>.
- [15] H. Paul, J. Sacher, *At. Data Nucl. Data Tables* **42** (1989) 105.
- [16] I. Orlic, C.H. Sow, S.M. Tang, *At. Data Nucl. Data Tables* **56** (1994) 159.
- [17] W. Brandt, G. Lapicki, *Phys. Rev. A* **23** (1981) 1717.
- [18] G. Lapicki, *Nucl. Instrum. and Meth. Phys. Res. B* **189** (2002) 820.
- [19] G. Lapicki, *Nucl. Instrum. and Meth. Phys. Res. B* **318** (2014) 6-10.

- [20] M. Pajek, D. Bana, J. Braziewicz, M. Czarnota, A. Bienkowski, M. Jaskla, A. Korman, D. Trautmann, and G. Lapicki, *Phys. Rev. A* **73** (2006) 012709.
- [21] D. Mitra, M. Sarkar, D. Bhattacharya, S. Santra, A.C. Mandal, G. Lapicki, *Nucl. Instrum. and Meth. Phys. Res. B* **268** (2010) 450459.
- [22] T. Mukoyama, *Nucl. Instrum. and Meth. Phys. Res. B* **354** (2015) 155-158.
- [23] J. Miranda, C.M. Romo-Krger, M. Lugo-Licona, *Nucl. Instrum. and Meth. Phys. Res. B* **189** (2002) 21.
- [24] M. Dingfelder, J.M. Fernandez-Varea, S. Segui, *J. Phys. Conf. Series* **194** (2009) 042001.
- [25] J.L. Campbell, J.-X. Wang, *At. Data Nucl. Data Tables* **43** (1983) 281.
- [26] J.L. Campbell, *At. Data Nucl. Data Tables* **85** (2003) 291; **95** (2009) 115.
- [27] J.E. Miraglia and M.S. Gravielle, *Phys. Rev. A* **78** (2008) 052705.
- [28] J.E. Miraglia, *Phys. Rev. A* **79** (2009) 022708.
- [29] J.E. Miraglia and M.S. Gravielle, *Phys. Rev. A* **81** (2010) 042709.
- [30] A.C. Tavares, C.C. Montanari, J.E. Miraglia, and G.M. Sigaud 2014, *J. Phys. B: At. Mol. Opt. Phys.* **47** (2014) 045201.
- [31] D.S.F. Crothers, J.F. McCann, *J. Phys. B* **16** (1983) 3229.
- [32] P.D. Fainstein, V.H. Ponce, and R.D. Rivarola, *J. Phys. B: At. Mol. Opt. Phys.* **21** (1988) 28799.
- [33] R.D. Rivarola, P.D. Fainstein, and V.H. Ponce, *Proc. 16th Int. Conf. on the Physics of Electronic and Atomic Collisions*, ed A Dalgarno et al (New York: AIP, 1989).
- [34] F. Salvat, J. M. Fernandez-Varea, and Jr W Williamson, *Comput. Phys. Comm.* **90** (1995) 151.
- [35] S. J. Cipolla, *Comp. Phys. Comm* **182** (2011) 2439-2440; **184** (2013) 2230-2231.
- [36] Z. Smit and G. Lapicki, *J. Phys. B: At. Mol. Opt. Phys.* **47** (2014) 055203.
- [37] M. Rodbro, E. Horsdal Pedersen, C. L. Cocke, and J. R. Macdonald, *Phys. Rev. A* **19** (1979) 1936.
- [38] C. L. Cocke, R. K. Gardner, B. Curnutte, T. Bratton and T. K. Saylor, *Phys. Rev. A* **16** (1977) 2248.
- [39] J. E. Golden and J. H. McGuire, *Phys. Rev. A* **15** (1977) 499.
- [40] N. Stolterfoht and D. Schneider, *Phys. Rev. A* **11** (1975) 721.
- [41] L.M. Winters, J.R. Macdonald, M.D. Brown, L.D. Ellsworth, and T. Chiao, *Phys. Rev. A* **7** (1973) 1276.
- [42] S.J. Czuchlewski, J.R. Macdonald, and L.D. Ellsworth, *Phys. Rev. A* **11** (1975) 1108.
- [43] W.M. Ariyasinghe, H.T. Awuku, and D. Powers, *Phys. Rev. A* **42** (1990) 3819-3825.
- [44] G. Schiwietz, U. Stettner, T.J.M. Zouros, N. Stolterfoht, *Phys. Rev. A* **35** (1987) 598.
- [45] N. Maeda, N. Kobayashi, H. Hori, M. Sakisaka, *J. Phys. Soc. Jap.* **40** (1976) 1430.
- [46] N. Stolterfoht, D. Schneider, P. Ziem, *Phys. Rev. A* **10** (1974) 81.
- [47] M.E. Rudd, *Phys. Rev. A* **10** (1974) 518.

[48] J.B. Crooks, M. E. Rudd, Phys. Rev. A **3** (1971) 1628

[49] R.L. Watson and L. H. Toburen Phys. Rev. A **7** (1973) 1853.

Explanation of Tables

To save space, throughout these tables the subindex $\pm n$ replaces the $10^{\pm n}$ factor.

Table 1. Total ionization cross sections, σ_{nlm} , of Neon K and L shells by 0.1-10 MeV protons. Atomic units are used.

E	proton impact energy in MeV
nlm	electron initial state
CDW-EIS	Total cross section per electron, σ_{nlm} , in atomic units, given by Eq. (1), with the CDW-EIS T-matrix element given by Eq. (3), for impact energies 0.1-1 MeV
Born	Total cross section per electron, σ_{nlm} , in atomic units, given by Eq. (1), with the first Born T-matrix element given by Eq. (2), for impact energies 1-10 MeV

Table 2. Total ionization cross sections, σ_{nlm} , of Argon K, L and M shells by 0.1-10 MeV protons. Atomic units are used. Explanation as in Table 1.

Table 3. Total ionization cross sections, σ_{nlm} , of Krypton L, M and N shells by 0.1-10 MeV protons. Atomic units are used. Explanation as in Table 1.

Table 4. Total ionization cross sections, σ_{nlm} , of Xenon M, N and O shells by 0.1-10 MeV protons. Atomic units are used. Explanation as in Table 1.

Table 5. Ionization probabilities at zero impact parameter of Neon K and L shells by 0.1-10 MeV protons.

E	proton impact energy in MeV
nlm	electron initial state
CDW-EIS	Ionization probability per electron at impact parameter $b = 0$, $P_{nlm}(0)$, given by Eq. (13), calculated within the CDW-EIS approximation as described in section 2, for impact energies 0.1-1 MeV
Born	Ionization probability per electron at impact parameter $b = 0$, $P_{nlm}(0)$, given by Eq. (13), calculated within the first Born approximation as described in section 2, for impact energies 1-10 MeV

Table 6. Ionization probabilities at zero impact parameter of Argon K, L and M shells by 0.1-10 MeV protons. Explanation as in Table 5.

Table 7. Ionization probabilities at zero impact parameter of Krypton M and N shells by 0.1-10 MeV protons. Explanation as in Table 5.

Table 8. Ionization probabilities at zero impact parameter of Xenon N and O shells by 0.1-10 MeV protons. Explanation as in Table 5.

Table 9. Mean radii $\langle r_{nl} \rangle$ of the atomic nl subshells of Ne, Ar, Kr and Xe (in atomic units).

Table 10. Impact parameter moment of order -1 , $\langle b_{nlm}^{-1} \rangle$ for 0.1-10 MeV protons in Ne, normalized to the inverse of the mean radio of each subshell, $\langle r_{nl} \rangle^{-1}$.

E	proton impact energy in MeV
nlm	electron initial state
CDW-EIS	Impact parameter moment of order -1 given by Eq. (14), calculated within the CDW-EIS approximation for impact energies 0.1-1 MeV
Born	Impact parameter moment of order -1 given by Eq. (14), calculated within the first Born approximation for impact energies 1-10 MeV

Table 11. Impact parameter moment of order -1 , $\langle b_{nlm}^{-1} \rangle$ for 0.1-10 MeV protons in Ar, normalized to the inverse of the mean radio of each subshell, $\langle r_{nl} \rangle^{-1}$. Explanation as in Table 10

Table 12. Impact parameter moment of order -1 , $\langle b_{nlm}^{-1} \rangle$ for 0.1-10 MeV protons in Kr, normalized to the inverse of the mean radio of each subshell, $\langle r_{nl} \rangle^{-1}$. Explanation as in Table 10

Table 13. Impact parameter moment of order -1 , $\langle b_{nlm}^{-1} \rangle$ for 0.1-10 MeV protons in Xe, normalized to the inverse of the mean radio of each subshell, $\langle r_{nl} \rangle^{-1}$. Explanation as in Table 10

Table 14. Impact parameter moment of order $+1$, $\langle b_{nlm}^1 \rangle$, for proton in Ne, normalized to the mean radio of each subshell, $\langle r_{nl} \rangle$.

E	proton impact energy in MeV
nlm	electron initial state
CDW-EIS	Impact parameter moment of order $+1$ given by Eq. (14), calculated within the CDW-EIS approximation for impact energies 0.1-1 MeV
Born	Impact parameter moment of order $+1$ given by Eq. (14), calculated within the first Born approximation for impact energies 1-10 MeV

Table 15. Impact parameter moment of order +1, $\langle b_{nlm}^1 \rangle$, for proton in Ar, normalized to the mean radio of each subshell, $\langle r_{nl} \rangle$. Explanation as in Table 14.

Table 16. Impact parameter moment of order +1, $\langle b_{nlm}^1 \rangle$, for proton in Kr, normalized to the mean radio of each subshell, $\langle r_{nl} \rangle$. Explanation as in Table 14.

Table 17. Impact parameter moment of order +1, $\langle b_{nlm}^1 \rangle$, for proton in Xe, normalized to the mean radio of each subshell, $\langle r_{nl} \rangle$. Explanation as in Table 14.

Table 10

Impact parameter moment of order -1 , $\langle b_{nlm}^{-1} \rangle$ for proton impact in Ne, normalized to the inverse of the mean radius of each subshell, $\langle r_{nl} \rangle^{-1}$. See page 14 for explanation.

Ne	CDW-EIS							Born					
E(MeV)	0.1	0.2	0.3	0.4	0.5	0.7	1	1	2	3	5	7	10
2p1	9.15 ₋₁	9.17 ₋₁	9.08 ₋₁	8.95 ₋₁	8.82 ₋₁	8.57 ₋₁	8.26 ₋₁	8.36 ₋₁	7.58 ₋₁	7.16 ₋₁	6.65 ₋₁	6.35 ₋₁	6.05 ₋₁
2p0	1.34	1.23	1.18	1.15	1.11	1.07	1.01	1.02	8.97 ₋₁	8.37 ₋₁	7.68 ₋₁	7.29 ₋₁	6.91 ₋₁
2s	1.19	1.17	1.20	1.23	1.25	1.29	1.31	1.32	1.31	1.29	1.25	1.23	1.19
1s	2.78	2.26	2.02	1.86	1.76	1.60	1.45	1.46	1.28	1.20	1.12	1.06	1.01

Table 11

Impact parameter moment of order -1 , $\langle b_{nlm}^{-1} \rangle$, for proton impact in Ar, normalized to the inverse of the mean radius of each subshell, $\langle r_{nl} \rangle^{-1}$. See page 14 for explanation.

Ar	CDW-EIS							Born					
E(MeV)	0.1	0.2	0.3	0.4	0.5	0.7	1	1	2	3	5	7	10
3p1	1.02	9.76 ₋₁	9.48 ₋₁	9.25 ₋₁	9.05 ₋₁	8.76 ₋₁	8.45 ₋₁	8.53 ₋₁	7.90 ₋₁	7.60 ₋₁	7.22 ₋₁	7.03 ₋₁	6.85 ₋₁
3p0	1.39	1.29	1.24	1.20	1.17	1.13	1.08	1.08	9.93 ₋₁	9.50 ₋₁	9.00 ₋₁	8.75 ₋₁	8.56 ₋₁
3s	1.37	1.48	1.55	1.57	1.58	1.59	1.59	1.60	1.58	1.56	1.53	1.51	1.48
2p1	1.60	1.45	1.37	1.31	1.26	1.21	1.16	1.16	1.07	1.02	9.60 ₋₁	9.18 ₋₁	8.73 ₋₁
2p0	2.27	2.32	2.21	2.13	2.06	1.94	1.80	1.73	1.48	1.36	1.23	1.15	1.08
2s	2.29	1.90	1.68	1.53	1.43	1.31	1.25	1.26	1.27	1.29	1.30	1.29	1.27
1s	3.38	3.17	2.81	2.58	2.44	2.22	2.02	2.03	1.68	1.53	1.38	1.31	1.23

Table 12

Impact parameter moment of order -1 , $\langle b_{nlm}^{-1} \rangle$, for proton impact in Kr, normalized to the inverse of the mean radius of each subshell, $\langle r_{nl} \rangle^{-1}$. See page 14 for explanation.

Kr	CDW-EIS							Born					
E(MeV)	0.1	0.2	0.3	0.4	0.5	0.7	1	1	2	3	5	7	10
4p1	1.15	1.09	1.06	1.03	1.01	9.83 ₋₁	9.53 ₋₁	9.47 ₋₁	8.88 ₋₁	8.55 ₋₁	8.15 ₋₁	7.91 ₋₁	7.68 ₋₁
4p0	1.62	1.48	1.42	1.38	1.35	1.31	1.26	1.25	1.16	1.12	1.06	1.03	9.99 ₋₁
4s	1.35	1.50	1.55	1.58	1.59	1.61	1.63	1.62	1.63	1.63	1.62	1.62	1.61
3d2	1.46	1.31	1.24	1.20	1.17	1.12	1.08	1.07	9.92 ₋₁	9.43 ₋₁	8.81 ₋₁	8.40 ₋₁	7.99 ₋₁
3d1	1.77	1.69	1.62	1.55	1.49	1.41	1.33	1.30	1.17	1.09	9.99 ₋₁	9.44 ₋₁	8.89 ₋₁
3d0	2.14	2.10	2.04	1.97	1.90	1.79	1.65	1.57	1.34	1.23	1.11	1.04	9.75 ₋₁
3p1	1.74	1.51	1.38	1.29	1.24	1.18	1.15	1.15	1.15	1.15	1.16	1.15	1.14
3p0	2.72	2.50	2.34	2.22	2.10	1.93	1.76	1.69	1.64	1.65	1.66	1.64	1.61
3s	2.29	1.90	1.70	1.56	1.49	1.44	1.46	1.44	1.45	1.44	1.41	1.39	1.36

Table 13

Impact parameter moment of order -1 , $\langle b_{nlm}^{-1} \rangle$, for proton impact in Xe, normalized to the inverse of the mean radius of each subshell, $\langle r_{nl} \rangle^{-1}$. See page 14 for explanation.

Xe	CDW-EIS							Born					
E(MeV)	0.1	0.2	0.3	0.4	0.5	0.7	1	1	2	3	5	7	10
5p1	1.15	1.11	1.07	1.05	1.03	9.99 ₋₁	9.68 ₋₁	9.72 ₋₁	9.13 ₋₁	8.84 ₋₁	8.52 ₋₁	8.36 ₋₁	8.21 ₋₁
5p0	1.62	1.55	1.49	1.44	1.40	1.35	1.30	1.31	1.22	1.18	1.15	1.12	1.10
5s	1.48	1.51	1.55	1.59	1.62	1.65	1.68	1.68	1.70	1.71	1.70	1.70	1.69
4d2	1.29	1.14	1.08	1.03	1.00	9.60 ₋₁	9.18 ₋₁	9.22 ₋₁	8.46 ₋₁	8.04 ₋₁	7.54 ₋₁	7.22 ₋₁	6.90 ₋₁
4d1	1.83	1.56	1.41	1.32	1.25	1.17	1.09	1.08	9.75 ₋₁	9.20 ₋₁	8.56 ₋₁	8.16 ₋₁	7.76 ₋₁
4d0	2.35	1.97	1.78	1.64	1.54	1.40	1.28	1.25	1.12	1.06	9.83 ₋₁	9.33 ₋₁	8.82 ₋₁
4p1	1.64	1.51	1.41	1.35	1.32	1.30	1.31	1.32	1.35	1.36	1.36	1.35	1.34
4p0	3.02	2.44	2.23	2.12	2.05	2.00	2.05	2.02	2.06	2.04	2.00	1.98	1.95
4s	1.98	1.79	1.71	1.69	1.69	1.73	1.73	1.65	1.63	1.64	1.62	1.60	1.57

Table 14Mean impact parameter, $\langle b_{nlm}^1 \rangle$, for proton in Ne, normalized to the mean radius of each subshell, $\langle r_{nl} \rangle$. See page 14 for explanation.

Ne	CDW-EIS							Born					
	0.1	0.2	0.3	0.4	0.5	0.7	1	1	2	3	5	7	10
E(MeV)													
2p1	1.85	1.91	2.00	2.09	2.17	2.33	2.53	2.53	3.06	3.44	4.03	4.49	5.05
2p0	1.42	1.58	1.69	1.80	1.90	2.08	2.31	2.33	2.92	3.35	4.01	4.51	5.11
2s	1.30	1.34	1.35	1.36	1.38	1.41	1.45	1.45	1.59	1.70	1.87	2.01	2.19
1s	6.02 ₋₁	7.33 ₋₁	8.24 ₋₁	9.00 ₋₁	9.60 ₋₁	1.06	1.18	1.18	1.37	1.47	1.62	1.73	1.86

Table 15Mean impact parameter, $\langle b_{nlm}^1 \rangle$, for proton in Ar, normalized to the mean radius of each subshell, $\langle r_{nl} \rangle$. See page 15 for explanation.

Ar	CDW-EIS							Born					
	0.1	0.2	0.3	0.4	0.5	0.7	1	1	2	3	5	7	10
E(MeV)													
3p1	1.55	1.67	1.79	1.90	2.00	2.16	2.36	2.35	2.82	3.06	3.46	3.68	3.88
3p0	1.28	1.44	1.58	1.70	1.81	2.00	2.23	2.22	2.74	3.01	3.44	3.66	3.87
3s	1.13	1.10	1.08	1.08	1.08	1.09	1.11	1.10	1.17	1.24	1.34	1.42	1.53
2p1	9.38 ₋₁	1.09	1.18	1.25	1.30	1.36	1.43	1.42	1.58	1.70	1.90	2.05	2.25
2p0	7.55 ₋₁	7.62 ₋₁	8.01 ₋₁	8.43 ₋₁	8.88 ₋₁	9.67 ₋₁	1.07	1.08	1.30	1.45	1.68	1.85	2.07
2s	6.96 ₋₁	8.39 ₋₁	9.50 ₋₁	1.03	1.10	1.11	1.23	1.21	1.28	1.32	1.40	1.47	1.55
1s	3.29 ₋₁	4.40 ₋₁	5.20 ₋₁	5.83 ₋₁	6.31 ₋₁	7.02 ₋₁	7.83 ₋₁	7.82 ₋₁	9.69 ₋₁	1.08	1.22	1.30	1.39

Table 16Mean impact parameter, $\langle b_{nlm}^1 \rangle$, for proton in Kr, normalized to the mean radius of each subshell, $\langle r_{nl} \rangle$. See page 15 for explanation.

Kr	CDW-EIS							Born					
	0.1	0.2	0.3	0.4	0.5	0.7	1	1	2	3	5	7	10
E(MeV)													
4p1	1.38	1.48	1.58	1.66	1.73	1.86	2.01	2.03	2.44	2.74	3.18	3.49	3.84
4p0	1.12	1.27	1.38	1.48	1.56	1.71	1.88	1.91	2.36	2.69	3.18	3.53	3.90
4s	1.10	1.07	1.05	1.04	1.04	1.04	1.04	1.05	1.07	1.09	1.12	1.16	1.20
3d2	1.15	1.31	1.38	1.43	1.47	1.53	1.60	1.64	1.85	2.00	2.25	2.46	2.70
3d1	9.59 ₋₁	1.02	1.09	1.16	1.21	1.29	1.39	1.44	1.68	1.86	2.15	2.37	2.64
3d0	8.46 ₋₁	8.86 ₋₁	9.41 ₋₁	9.99 ₋₁	1.05	1.15	1.26	1.34	1.62	1.82	2.12	2.35	2.63
3p1	8.33 ₋₁	9.85 ₋₁	1.09	1.16	1.21	1.26	1.29	1.46	1.54	1.58	1.65	1.71	1.80
3p0	6.43 ₋₁	7.03 ₋₁	7.41 ₋₁	7.78 ₋₁	8.18 ₋₁	8.90 ₋₁	9.64 ₋₁	1.19	1.33	1.42	1.55	1.64	1.75
3s	6.69 ₋₁	7.99 ₋₁	9.01 ₋₁	9.80 ₋₁	1.03	1.09	1.11	1.09	1.13	1.16	1.21	1.26	1.33

Table 17Mean impact parameter, $\langle b_{nlm}^1 \rangle$, for proton in Xe, normalized to the mean radius of each subshell, $\langle r_{nl} \rangle$. See page 15 for explanation.

Xe	CDW-EIS							Born					
	0.1	0.2	0.3	0.4	0.5	0.7	1	1	2	3	5	7	10
E(MeV)													
5p1	1.33	1.44	1.53	1.62	1.69	1.81	1.95	1.94	2.25	2.44	2.65	2.77	2.89
5p0	1.09	1.22	1.33	1.43	1.51	1.65	1.81	1.81	2.15	2.35	2.57	2.70	2.81
5s	1.03	1.02	1.01	1.00	1.00	9.99 ₋₁	9.99 ₋₁	9.93 ₋₁	1.01	1.02	1.04	1.06	1.08
4d2	1.17	1.32	1.40	1.47	1.53	1.62	1.74	1.73	2.03	2.26	2.61	2.88	3.20
4d1	9.14 ₋₁	1.06	1.17	1.26	1.33	1.45	1.59	1.58	1.92	2.16	2.54	2.83	3.19
4d0	8.01 ₋₁	9.48 ₋₁	1.05	1.14	1.22	1.35	1.50	1.50	1.86	2.12	2.51	2.81	3.18
4p1	8.20 ₋₁	9.22 ₋₁	1.01	1.06	1.09	1.11	1.12	1.11	1.14	1.16	1.20	1.23	1.29
4p0	5.81 ₋₁	6.80 ₋₁	7.27 ₋₁	7.64 ₋₁	7.93 ₋₁	8.32 ₋₁	8.48 ₋₁	8.52 ₋₁	8.77 ₋₁	9.02 ₋₁	9.55 ₋₁	1.00	1.07
4s	7.11 ₋₁	7.86 ₋₁	8.54 ₋₁	9.02 ₋₁	9.27 ₋₁	9.42 ₋₁	9.49 ₋₁	9.64 ₋₁	9.91 ₋₁	1.02	1.07	1.11	1.17